RSC Advances

ROYAL SOCIETY OF CHEMISTRY

PAPER

View Article Online
View Journal | View Issue

Check for updates

Cite this: *RSC Adv.*, 2022, **12**, 7671

Ag_3VO_4/g-C_3N_4/diatomite ternary compound reduces Cr(VI) ion in aqueous solution effectively under visible light

Zhuhuan Jiang,†[ad] Haitao Zhu,†[b] Wanmi Guo, *[acd] Qifang Ren,[acd] Yi Ding,*[acd] Shaohua Chen,[b] Jing Chen[d] and Xinyu Jia[d]

Received 23rd December 2021
Accepted 23rd February 2022

DOI: 10.1039/d1ra09295b

rsc.li/rsc-advances

In recent years, the conversion of Cr(VI) to Cr(III) ions by semiconductor photocatalysis technology has been considered to be an effective method to solve this problem. In this paper, a kind of ternary composite, Ag_3VO_4/g-C_3N_4/diatomite (AVO/CN/DT), was synthesized by a two-step method (annealing–precipitation). Through a series of characterization analyses, the crystal morphology, microstructure, optical properties and photoelectrochemical properties of the material were characterized and analyzed. The band edge of g-C_3N_4 was red-shifted due to the addition of Ag_3VO_4 and diatomite. Consequently, the visible light response of the composites was intensified. Taking Cr(VI) in aqueous solution as a target pollutant, the degradation efficiency using 4AVO/CN/0.06DT reached 70% within 60 min under visible light irradiation, far exceeding the degradation efficiency using the pure substances. The cyclic degradation performance of the composite material was tested, and it still had a stable degradation effect after three cycles. The degradation efficiency in solution at different pH values was investigated. When the pH value of the solution gradually increased, the degradation efficiency gradually decreased, which was mainly caused by the different forms of Cr(VI) under different pH values. A corresponding degradation mechanism was proposed. Diatomite provided a reaction site for Ag_3VO_4 and g-C_3N_4, which promoted the photoreduction of Cr(VI). This work provides some reference significance for deepening the application field of diatomite and treating heavy metal ion wastewater.

1. Introduction

Nowadays, people pay more and more attention to the problem of environmental pollution, especially toxic heavy metal ions in water, which is directly related to the life and health of human beings. Among the pollutants discharged from industry, hexavalent chromium usually exists in the wastewater from chromate production, electroplating, lacquer making, leather tanning and other industries.[1–4] Hexavalent chromium (Cr(VI)) is easily absorbed by the human body, entering through digestion, the respiratory tract, skin and other ways. It accumulates in organisms and can lead to cancer. The toxicity of Cr(VI) poses a significant threat to human health.[5–7] Studies have shown that when Cr(VI) is reduced to Cr(III), the toxicity of chromium can be greatly reduced.[8,9] Since solar semiconductor photocatalytic technology has the advantages of sustainability, non-toxicity, low cost and environmental protection, it has received extensive attention.[10–12] Using semiconductor photocatalytic technology to convert Cr(VI) to Cr(III) is an ideal method to solve this problem. It is particularly important to design and construct effective photocatalytic materials for Cr(VI) reduction. In recent years, many researchers have successfully constructed reasonable semiconductor photocatalytic materials to effectively photoreduce Cr(VI) to Cr(III).[13] For example, Yi *et al.* reported a new *Z*-scheme g-C_3N_4/UIO-66 heterojunction photocatalyst prepared by the ball milling method, which was composed of two-dimensional g-C_3N_4 and 3D UIO-66 heterojunction photocatalyst. It has excellent photoreducing ability for Cr(VI) in solution.[8]

Diatomite (DT) is a kind of porous siliceous sedimentary rock formed by the remains of ancient diatoms.[14,15] Among naturally occurring materials, DT has excellent characteristics such as high porosity, high permeability, small particle size, high surface area, low thermal conductivity and chemical inertia.[16,17] DT is an excellent photocatalyst carrier material due to its wide distribution, abundant reserves and low price in China.[18,19] The abundant micro-/nanostructure on the surface of DT can provide a good composite anchor point for catalytic

---

[a] Anhui Province International Research Center on Advanced Building Materials, Anhui Jianzhu University, Hefei 230022, Anhui, China

[b] Technology Center of Hefei Customs District, Hefei 230022, Anhui, China

[c] Anhui Provincial Key Laboratory of Environmental Pollution Control and Resource Reuse, Anhui Jianzhu University, Hefei 230022, Anhui, China

[d] Anhui Province Key Laboratory of Advanced Building Materials, Anhui Jianzhu University, Hefei 230022, Anhui, China. E-mail: 17856178532@139.com; dyrqf@ahjzu.edu.cn; Fax: +86-0551-63828106; Tel: +86-0551-63828151

† These authors contributed equally to this work.

particles, which is conducive to the uniform dispersion of catalytic particles and the reduction of polymerization between particles, thus increasing the active sites of catalytic reaction.[20,21] DT-based composite photocatalytic materials often have excellent adsorption performance, which can effectively improve the contact probability between a catalyst and pollutants and improve the photocatalytic degradation activity, which is also conducive to overcome the difficult adsorption of pollutants due to the small specific surface area of the catalyst.[22,23] Tanniratt *et al.* used zinc dust waste and DT waste extracted from the beer industry as raw materials to load ZnO particles onto DT carrier through a simple impregnation and calcination method, successfully improving the photocatalytic activity of ZnO and realizing efficient reuse of waste.[24]

Among the widely studied photocatalytic semiconductor materials, graphite-like carbon nitride (g-C_3N_4) (about 2.70 eV) has attracted a lot of attention due to its simple preparation process and certain response in the visible spectrum range.[25–27] However, its poor optical response performance and low quantum efficiency are still problems that must be solved.[28] In order to apply carbon nitride in the field of photocatalysis and energy as soon as possible, it is urgent to improve its photocatalytic efficiency.[29] To date, many methods have been explored to improve the photocatalytic performance of g-C_3N_4, including liquid-phase stripping,[30] alkaline treatment of g-C_3N_4,[31] element doping[32] and coupling with other photocatalysts.[33] Among these methods, coupling with other semiconductors is an effective and simple method, which can improve the separation efficiency of photogenerated electrons and holes, and is widely used. For example, g-C_3N_4–CdS,[34] g-C_3N_4–ZnO[35] and other photocatalysts have shown high catalytic activity. Due to its relatively narrow band gap and wide response range to visible light, Ag_3VO_4 has attracted much attention for its excellent performance in decomposing organic pollutants, antibacterial activity and water decomposition under visible light irradiation.[36,37] Although pure Ag_3VO_4 shows excellent photocatalytic activity, its quantum yield is relatively low. In order to overcome the above shortcomings, many attempts have been made to improve the separation of photoinduced carriers.[38,39] The two-dimensional nanostructure of g-C_3N_4 has a large specific surface area, which can effectively transfer photogenerated electrons and improve the photogenerated quantum yield, such as Bi_2WO_6/g-C_3N_4,[40,41] g-C_3N_4/AgBr.[42] Based on previous studies, we modified Ag_3VO_4 with g-C_3N_4 to form a new composite material for further study of its photocatalytic activity.

In the present work, a novel ternary Ag_3VO_4/g-C_3N_4/diatomite composite photocatalyst was synthesized by a two-step method using natural DT as the base material. Through the related characterization, the crystal phase, morphology, optical properties and electrochemical properties of the composite material were comprehensively analyzed. Cr(VI) in aqueous solution was used as a target degradable substance, and Cr(VI) was converted into Cr(III) under the condition of light to reduce the toxicity of chromium ions. In addition, the reduction process of Cr(VI) and the transformation mechanism of Cr(III) were studied in depth, which provided a new method for the further utilization of DT and the removal of heavy metal ions from industrial pollution.

2. Experimental section

2.1. The synthesis of Ag_3VO_4/g-C_3N_4/diatomite

Ag_3VO_4/g-C_3N_4/diatomite composite material was prepared by a two-step method. The specific steps were as follows: DT (0.02 g, 0.04 g, 0.06 g, or 0.1 g) was weighed into 30 mL methanol solution and dispersed by ultrasonication for 0.5 h to obtain a suspension of DT. 4 g of urea was added and stirred vigorously for 1 h. The product was moved to an air-blast drying oven and dried for 8 h at 60 °C. The product was fully ground and moved to an alumina crucible, wrapped tightly with tin foil paper, and calcined in a muffle furnace at high temperature. The calcination process is the same as in the preparation of g-C_3N_4 (preparation of g-C_3N_4: urea was heated to 80 °C at 5 °C min^{-1} in a muffle furnace and held for 2 h, then heated to 580 °C at 5 °C min^{-1} and held for 2 h). After calcination, the product was fully crushed, ultrasonically dispersed with ethanol for 8 h, and the product was dried to obtain g-C_3N_4/diatomite material. 0.2 g g-C_3N_4/diatomite was added into 20 mL water and super dispersed for 0.5 h. Then, 0.155 g of solid $AgNO_3$ was weighed into 30 mL water and magnetically stirred for 0.5 h in the dark. The Ag^+ solution was added to the suspension of g-C_3N_4/diatomite material and magnetically stirred in the dark for 1 h. Then, 0.056 g of solid Na_3VO_4 was weighed into 30 mL of water and magnetically stirred until the solution was clear and transparent. The Ag^+/g-C_3N_4/diatomite solution was then added dropwise to Na_3VO_4 solution while stirring vigorously. After complete addition, NaOH (0.1 M) was used to adjust the pH value of the solution to 11, and the solution was continued to be stirred in the dark for 3 h. After stirring, the product was centrifugally washed, washed alternately with ethanol and deionized water for 5 times, then placed in a drying oven and dried at 70 °C for 10 h. The products were labeled as 4AVO/CN/0.02DT, 4AVO/CN/0.04DT, 4AVO/CN/0.06DT, and 4AVO/CN/0.1DT according to the quantity of added DT.

2.2. Characterizations

The crystal structure of samples was characterized by powder X-ray diffraction (TD-3000) with Cu–K radiation (λ = 0.1541874 nm) at an angle of 10–70°. FT-IR spectra were recorded with a Thermo Nicolet IS10 FTIR analyzer, and KBr was used as reference. The morphology of the samples was characterized with a JEOL-7500B field emission scanning electron microscope and a JEOL-2010 transmission electron microscope. X-ray photoelectron spectroscopy (XPS) analysis was performed with an Escalab-250xi system. Solid UV-visible spectra were measured with an SP-752 spectrophotometer. Photoluminescence (PL) spectroscopy was performed using a Hitachi F-4700 with excitation wavelength at 350 nm. A Chi 660E electrochemical workstation was used for photochemical characterization. Ag/AgCl and Pt were used as control electrodes, and 0.5 M Na_2SO_4 solution was used as electrolyte. Electron spin resonance (ESR) was measured with a Bruker A-300 spectrometer, and DMPO was used to capture free radical signals during photocatalysis.

2.3. Photocatalytic experiments

In the photocatalytic experiments, a 500 W xenon lamp (Beijing Zhongjiaojinyuan Company) with a 420 nm cutoff filter was used as the light source for irradiation. The concentration change of Cr(VI) was used as the expression of the degradation effect of catalyst. A UV-visible light spectrophotometer (UV-5500PC) was used to measure the absorbance value of Cr(VI) in solution at a wavelength of 350 nm.[43,44] 50 mg photocatalyst was added to 100 mL potassium dichromate solution (10 mg L^{-1}, pH = 2) and stirred for 30 min under dark conditions to achieve adsorption–dissolution equilibrium. Then, every 10 min, 4 mL of the suspension was extracted with a syringe under light conditions, and the solution to be tested was separated with a 0.22 μm microporous filter membrane. The absorbance value of the solution was measured with a UV-visible light spectrophotometer. The initial pH value of the solution has an obvious effect on the degradation of Cr(VI). A series of Cr(VI) solutions with different initial pH values were prepared for degradation to explore the best pH value. The stability of the photocatalyst is an important index to evaluate the material, and the material is degraded in three cycles.

3. Results and discussion

The XRD patterns of samples are shown in Fig. 1. It can be seen that the characteristic peak of pure DT is at 26.7° from Fig. 1a, which is the characteristic peak of opal.[18] The characteristic peaks of pure CN (JCPDS no. 87-1526) are $2\theta = 13.1°$ and $2\theta = 27.74°$, corresponding to plane (100) and plane (002), respectively.[35] The XRD pattern of CN/0.06DT composite synthesized by impregnation and calcination method was obtained, the characteristic peaks of DT and carbon nitride successfully appeared, there were no other impurity peaks, and the surface of the two were successfully combined. The main characteristic peaks of the synthesized Ag_3VO_4 (AVO) in Fig. 1b appear at $2\theta = 32.7°$ and $2\theta = 33.8°$ corresponding to the (−121) and (121) crystal planes of Ag_3VO_4, respectively, which correspond to the standard card of Ag_3VO_4 (JCPDS no. 43-0542). As shown in Fig. 1b, the XRD pattern of 4AVO/CN/0.06DT ternary composite successfully showed characteristic peaks of DT, g-C_3N_4 (CN) and AVO, and no other impurity peaks appeared, indicating that the presence of the three did not change the crystal structure of the material, nor did they bring about other impurity phase peaks. The results show that the synthesis of the composite is successful.

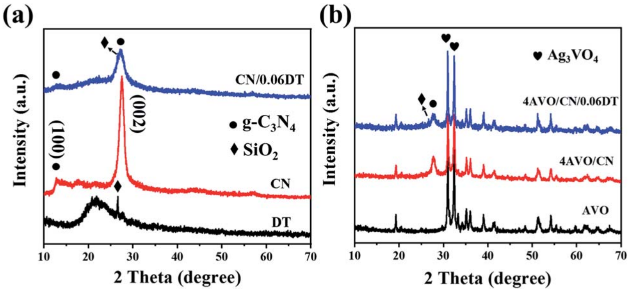

Fig. 1 XRD patterns of the sample (a) DT, CN and CN0.06DT and (b) AVO, 4AVO/CN and 4AVO/CN/0.06DT.

The functional groups of the prepared samples were analyzed by infrared spectroscopy. Fig. 2 shows the infrared spectra of the prepared samples. In the infrared spectrum of DT, the strong band at 1054 cm^{-1} and the two bands at 796 and 468 cm^{-1} correspond to asymmetric tensile vibration, symmetric tensile vibration and bending vibration of Si–O–Si bond, respectively, which are characteristic peaks of DT.[45] In Fig. 2, the peak of the infrared spectrum of pure CN at 808 cm^{-1} corresponds to the stretching vibration of the structural unit of triazine ring.[46] The absorption peak between 1650 and 1200 cm^{-1} can be expressed as the stretching vibration peak of triazine ring structure skeleton.[35,47] In addition, the absorption band from 3500 cm^{-1} to 3000 cm^{-1} corresponds to the stretching vibration of the terminal NH_2 and the NH groups generated by the incomplete condensation of CN. In the infrared spectrum of pure AVO, the peak at 875 cm^{-1} corresponds to V═O double bond vibration.[48,49] As can be seen from the infrared spectra, the absorption peaks of the composites CN/0.06DT, 4AVO/CN and 4AVO/CN/0.06DT are consistent with those of the above prepared samples.

The microstructure of the prepared material was observed by SEM and TEM. Fig. 3a shows the SEM image of DT. It can be observed that the microscopic morphology of DT is disk-like, and the surface is distributed with holes of uniform size. Such structure has good adsorption effect. Fig. 3b shows CN prepared by calcination method. It can be seen that after a long time of ultrasonic stripping, the carbon nitride presents a lamellar structure, which is stacked layer by layer, greatly improving the specific surface area of the carbon nitride. As can be seen from Fig. 3c, the size of AVO nanoparticles is uniform, but the agglomeration phenomenon is serious, which greatly limits the activity of AVO. Fig. 3d shows the scanning image of 4AVO/CN/0.06DT composite material. It can be seen that carbon nitride

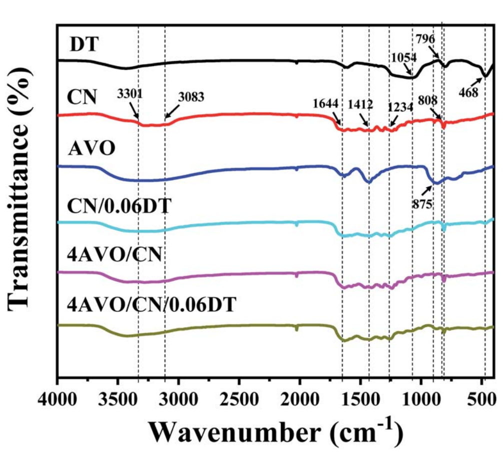

Fig. 2 Infrared spectra of samples.

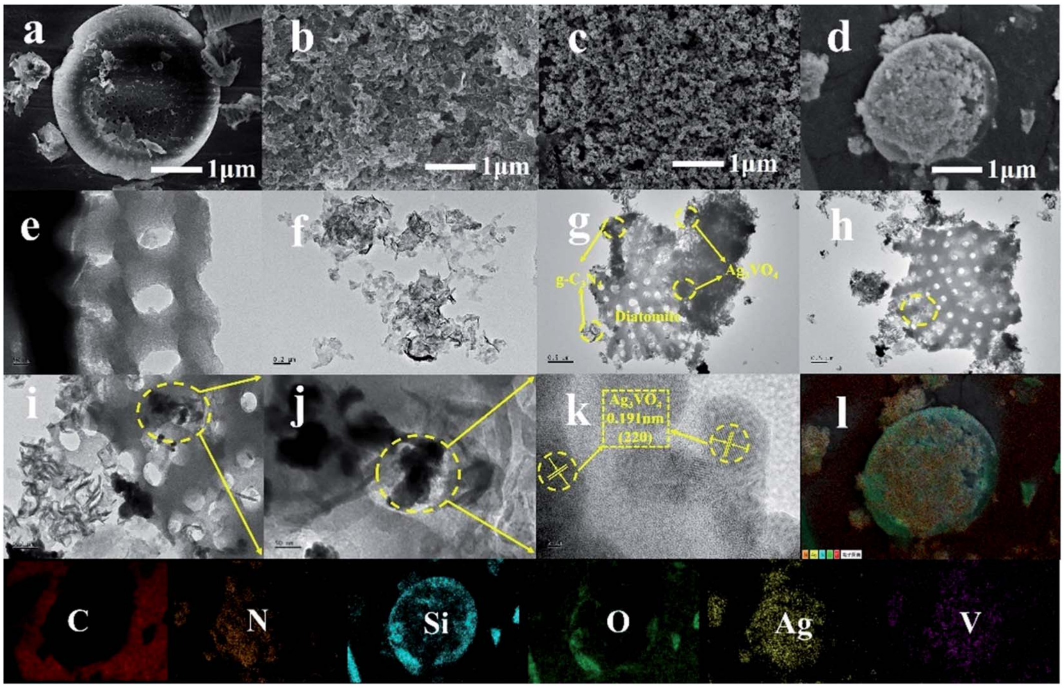

Fig. 3 Scanning images of (a) DT, (b) CN, (c) AVO and (d) 4AVO/CN/0.06DT. Transmission images of (e) DT, (f) CN, and (g)–(j) 4AVO/CN/0.06DT and high-resolution image of (k) 4AVO/CN/0.06DT. (l) Mapping of C, N, Si, O, Ag, V elements of 4AVO/CN/0.06DT composite.

nanosheets and a large number of AVO nanoparticles were attached to the disc of DT, indicating that the composite material was successfully prepared by the impregnation–deposition–roasting method. In order to further observe the morphological characteristics of the material, we used transmission electron microscopy for characterization. Fig. 3e and f show the transmission images of DT and CN respectively. It can be seen that the surface of DT has a uniformly distributed pore structure of the same size. The carbon nitride stripped by ultrasound also showed a lamellar morphology, and the specific surface area was greatly increased. Fig. 3g–j show transmission images of 4AVO/CN/0.06DT composite material. It can be seen that there are a large number of lamellar carbon nitride nanosheets attached to the disc of DT. Due to the localized effect of large surface area of carbon nitride and DT, AVO nanoparticles are uniformly distributed on the disc of carbon nitride and DT, and the agglomeration effect is significantly improved. This is consistent with the results of scanning electron microscope imaging. Fig. 3k shows a high-resolution transmission image of 4AVO/CN/0.06DT composite material. After analysis, the spacing of lattice fringes is 0.191 nm, corresponding to the (220) plane of Ag_3VO_4.[48] In addition, in order to observe the elemental distribution of the composite material, we used SEM mapping to observe the distribution of each element. The results are shown in Fig. 3l. The six elements C, N, Si, O, Ag and V are evenly distributed, indicating the successful preparation of the composite material.

XPS can be used to characterize the elemental composition and bond type of the samples. A sample of 4AVO/CN/0.06DT was investigated by XPS, and the individual peaks of each component of the sample can be seen in Fig. 4. Fig. 4a shows the full element spectrum of the sample, and it can be seen that all the elements O, C, N, Ag, V and Si contained in the sample appear in the spectrum. Fig. 4b shows the 1s peak display map of O, and it can be seen that there are three groups of peaks, 530.40 eV, 531.63 eV and 533.11 eV respectively, corresponding to V–O bond in Ag_3VO_4, O in the surface hydroxyl group and Si–O bond in DT.[38,47] Fig. 4c shows a 1s high-resolution map of C, showing three groups of peaks at 284.5 eV, 286.2 eV, and 287.3 eV, respectively, corresponding to the characteristic bond type of graphite carbon (C–C), the C–NH_2 bond of C and sp^2 hybrid carbon atom bonded to N in aromatic ring (C=N).[7,36] Three groups of peaks can be observed in the N 1s high-resolution map (Fig. 4d), and the peak values of these three groups are 398.06 eV, 399.08 eV, and 400.61 eV respectively: 398.06 eV corresponds to sp^2 hybrid nitrogen in the triazine ring (C=N–C); 399.4 eV to the third N atom in the N–$(C)_3$ group; 400.7 eV to the characteristic peak of amino nitrogen (N–H).[50] Fig. 4e shows a high-resolution map of the 3d orbital of Ag, showing two sets of peaks, 368.67 eV and 374.74 eV, corresponding to the $3d_{5/2}$ and $3d_{3/2}$ orbitals of Ag.[48] Fig. 4f shows a high-resolution display map of V element. Peaks at 516.38 eV and 523.73 eV correspond to the $2p_{3/2}$ and $2p_{1/2}$ orbitals of V, respectively. From the above analysis, it can be seen that DT, CN and AVO are bonded together by chemical bonds rather than simple physical mixing, which also proves the successful preparation of 4AVO/CN/0.06DT composites.

UV-vis-DRS was used to study the optical absorption properties of the prepared materials. As shown in Fig. 5a, compared with CN, AVO and composite materials, DT has the lowest light absorption rate, which may be attributed to the light scattering effect generated by the composition and structure of natural minerals.[18] For CN and AVO, the visible light absorption boundaries are

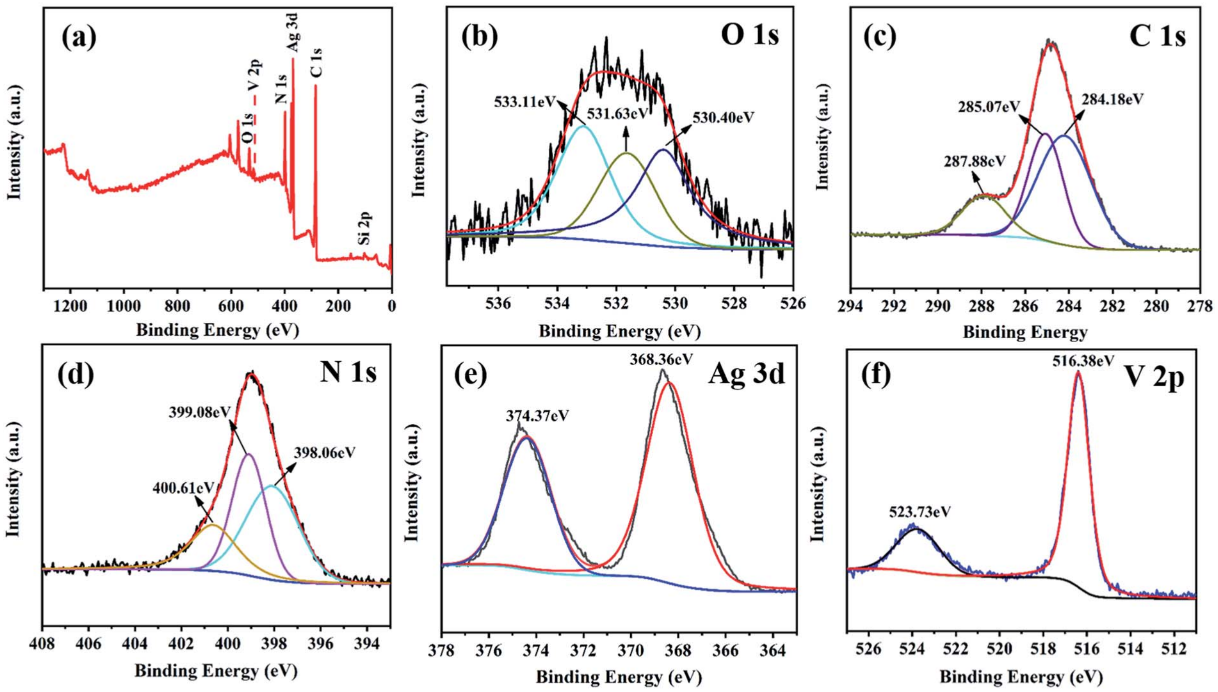

Fig. 4 XPS spectra of 4AVO/CN/0.06DT.

about 456 nm and 578 nm. The absorption boundary of the 4AVO/CN composite has a certain red shift, which is about 595 nm, compared with that of CN and AVO. But the absorption intensity is reduced. This may be because the addition of DT has a certain dispersion effect on photosensitive particles, resulting in the red shift of the absorption boundary of the sample. In addition, DT has a poor absorption of light, so the absorption intensity of the composite material decreases. According to the band gap width plot in Fig. 5b, for direct and indirect gap semiconductors, the value of n is 1/2 and 2, respectively. AVO and CN are direct gap semiconductors, so the value of n here is 1/2. As shown in Fig. 5b, the values of E_g of AVO and CN were 2.10 eV and 2.70 eV, respectively, which are almost the same as previous reports.[51,52] The band gaps of 4AVO/CN and 4AVO/CN/0.06DT composites are 2.46 eV and 2.30 eV, respectively.

The photoreduction of Cr(VI) by various catalysts under visible light was studied. In the absence of light or catalyst, there is no photoreduction. Under visible light irradiation with 4AVO/CN/0.06DT, the photoreduction rate of hexavalent chromium is 70% within 60 min, and the photoreduction rates with CN, AVO, DT and AVO/CN are 8%, 3%, 1% and 49%, respectively (Fig. 6a and b). Fig. 6c shows the photoreduction performance of 4AVO/CN/0.06DT for Cr(VI) at different initial pH. When the initial pH value gradually increases, the degradation efficiency of the photoreductant decreases rapidly, which is mainly due to the different existing forms and reaction principles of Cr(VI) in aqueous solution with different pH values.[6] Related studies indicate that under acidic conditions, Cr(VI) mainly exists in the form of HCrO$_7^-$, and H$^+$ in the solution needs to be consumed in the process of converting Cr(VI) to Cr(III). According to Le

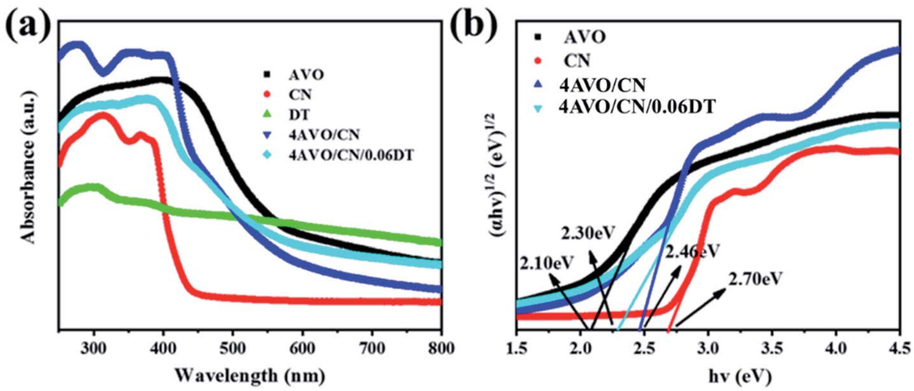

Fig. 5 (a) UV-vis-DRS spectra of DT, AVO, CN, 4AVO/CN and 4AVO/CN/0.06DT. (b) Band-gap width diagrams for AVO, CN, 4AVO/CN and 4AVO/CN/0.06DT.

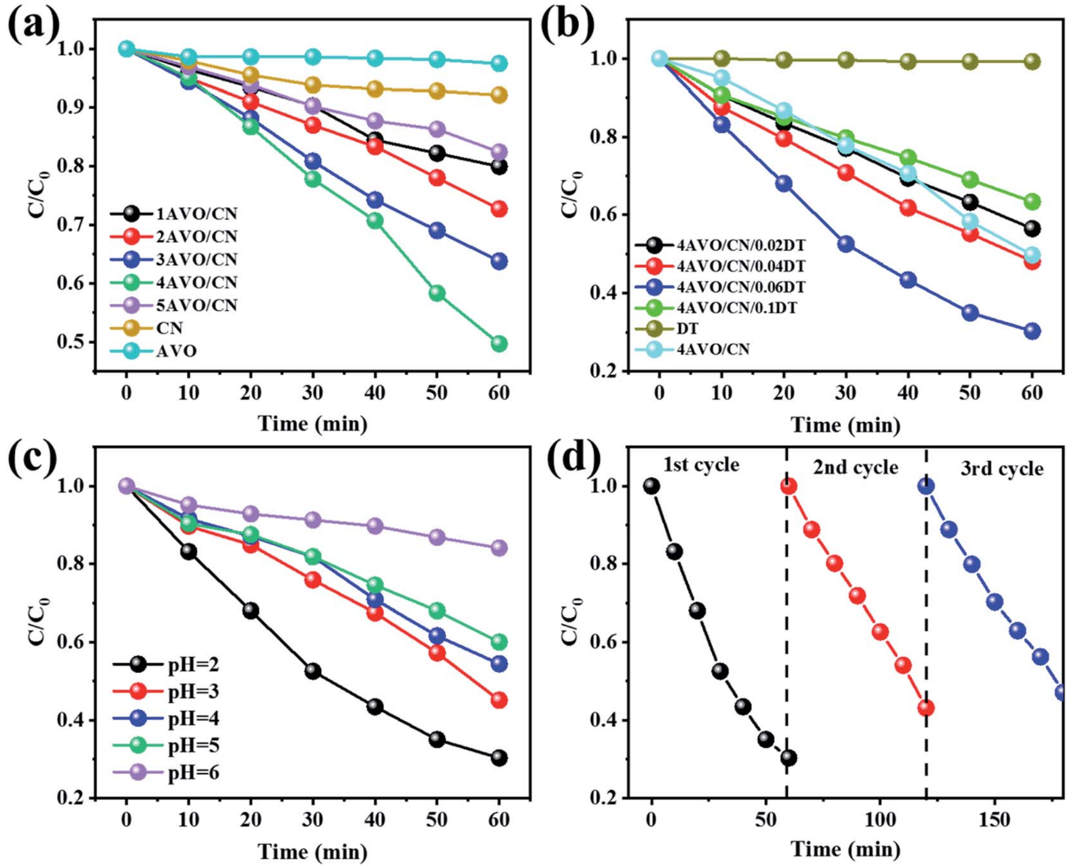

Fig. 6 (a and b) Degradation renderings of Cr(VI) for samples of CN, AVO, DT, *x*AVO/CN and 4AVO/CN/*x*DT. (c) The effect of pH value on Cr(VI) degradation. (d) Cyclic degradation diagram of 4AVO/CN/0.06DT sample.

Chatelier's principle, H^+ in strong acidic solution can promote the conversion of Cr(VI) to Cr(III), and promote the reaction to move in the positive direction. Under alkaline conditions, Cr(VI) mainly exists in aqueous solution in the form of CrO_4^{2-}. In the process of producing Cr(III), OH^- ions will be generated, and the decrease of solution acidity will inhibit the forward movement of the reaction.[53,54] Moreover, the generated $Cr(OH)_3$ precipitate will be deposited on the surface of the photocatalyst, blocking the active sites and further restricting the photocatalytic reduction of Cr(VI).[55] The photocatalytic performance of 4AVO/CN/0.06DT ternary material decreased to a certain extent after three cyclic degradation tests, which may be caused by the loss of photocatalyst during sample recovery.

The electron–hole pair recombination efficiency of CN, AVO and 4AVO/CN/0.06DT was determined by the PL technique. The higher the fluorescence intensity value, the greater the recombination rate of electron–hole pairs, and the lower the photocatalytic activity. As shown in Fig. 7a, CN is excited at 350 nm and has a strong excitation peak around 435 nm. For pure AVO, the intensity of the excitation peak at a similar position is much lower than that of pure CN. The PL spectrum of 4AVO/CN/0.06DT ternary composite is similar to that of pure AVO, but its strength also decreases obviously. PL results clearly show that the electron–hole pair recombination rate of 4AVO/CN/0.06DT ternary composite is much lower than that of pure CN and AVO, which indicates that its photocatalytic performance is the best. In order to further investigate the effect of heterojunction formation on the enhancement of photocatalytic activity, electrochemical impedance spectroscopy (EIS), photocurrent and Mott–Schottky curves were used to study the photochemical properties of the products. EIS is an effective technique to study the charge transfer efficiency on electrodes. Generally speaking, the smaller the arc radius, the higher the charge transfer efficiency, which is attributed to the smaller charge transfer resistance on the electrode surface.[6] Fig. 7b shows the EIS results of CN, AVO and 4AVO/CN/0.06DT samples. The EIS changes of CN, AVO and 4AVO/CN/0.06DT are seen in the figure. This indicates that 4AVO/CN/0.06DT composite can promote the transfer of photoelectric charge across the interface of the semiconductor hybrid material, thus improving its photocatalytic activity. Fig. 7c shows the response curve of photocurrent over time of photocatalysts. All the photoelectrodes showed stable photoelectric response for four switching cycles under light. The photocurrent density of 4AVO/CN/0.06DT ternary composite is obviously higher than that of pure CN and AVO, which indicates that the photoelectric separation efficiency of the composite has been significantly improved. Fig. 7d shows the Mott–Schottky curves of CN, AVO and 4AVO/CN/0.06DT composite. This is a typical n-type semiconductor characteristic profile. The conduction band (CB)

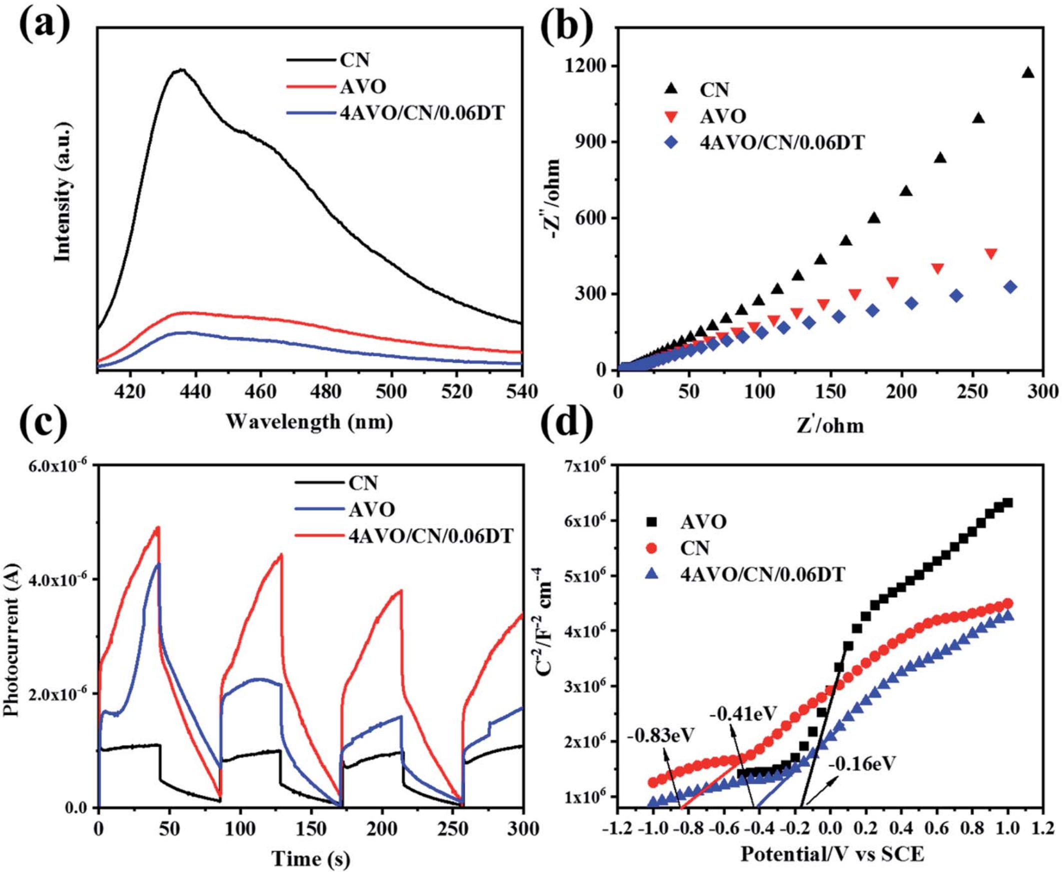

Fig. 7 (a) PL emission spectra of CN, AVO and 4AVO/CN/0.06DT samples. (b) Electrochemical impedance spectroscopy results of CN, AVO and 4AVO/CN/0.06DT samples. (c) Photocurrent chromatograms of CN, AVO and 4AVO/CN/0.06DT samples and (d) Mott–Schottky chromatograms of CN, AVO and 4AVO/CN/0.06DT samples.

values of CN, AVO and 4AVO/CN/0.06DT can be determined by the intersection of the tangent line of the curve and the horizontal axis, and the values of the three are −0.83 eV, −0.16 eV and −0.41 eV, respectively.

In order to determine the main active species of 4AVO/CN/0.06DT composite in the process of photocatalytic reduction of Cr(VI) and understand the reaction principle, we used ESR to determine the active species of composites. As shown in Fig. 8a and b, $^{\bullet}O_2^-$ and $^{\bullet}OH$ characteristic ESR signals were detected in solution under the irradiation of white light, and the signals of both were significantly strong. But in the dark, no signal was detected, indicating that no active substance was formed in the absence of light.

In summary, the degradation mechanism of Cr(VI) in photocatalytic reduction by 4AVO/CN/0.06DT ternary composite was proposed, as shown in Fig. 9. In the photocatalytic reaction

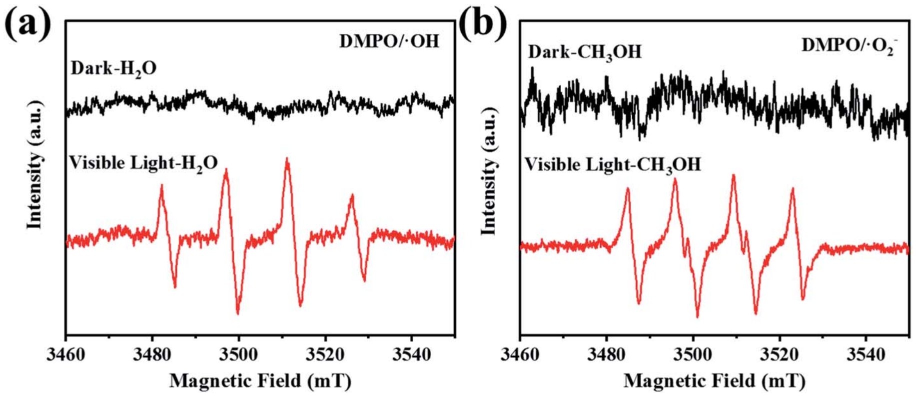

Fig. 8 ESR spectra of the captured active substances: (a) $^{\bullet}OH$ radical and (b) $^{\bullet}O_2^-$ radical of 4AVO/CN/0.06DT composite.

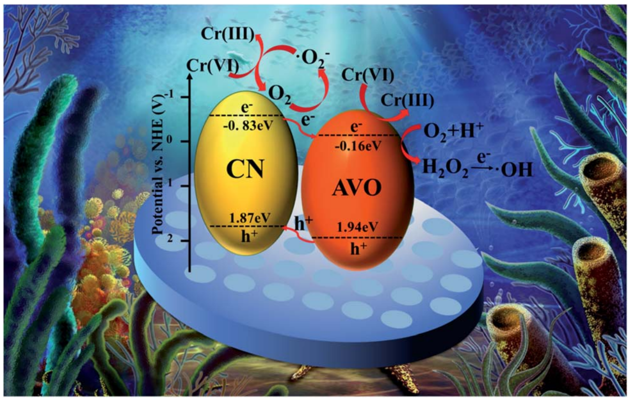

Fig. 9 Degradation mechanism diagram of Cr(VI) by 4AVO/CN/0.06DT composite.

system, DT, as the matrix material, provides the reaction interval, and the excellent pore structure of DT has a good adsorption effect on degradable pollutants in solution, which promotes the reaction to a certain extent.[18,23] According to the above UV-vis-DRS and photoelectrochemical analysis, the band gaps of CN, AVO and 4AVO/CN/0.06DT are 2.70 eV, 2.10 eV and 2.30 eV. The valence band (VB) edge energy can be obtained from $E_{\mathrm{VB}} = E_{\mathrm{CB}} + E_{\mathrm{g}}$. Their VB values are 1.87 eV, 1.94 eV and 1.89 eV, respectively. CB values are −0.83 eV, −0.16 eV and −0.41 eV, respectively. As can be seen from the figure, the VB value of CN is lower than that of AVO, and the photogenerated hole is transferred to the lower VB of CN. Since the VB value of AVO is 2.27 eV, which is basically equal to the standard reaction potential of $H_2O/{}^{\bullet}OH$ radical of 2.27 eV, $^{\bullet}OH$ is generated by the reaction with water in the process of illumination.[8] The CB value of CN is −0.80 eV lower than the CB value of AVO of −0.11 eV. The generation of photogenerated electrons will move to a higher potential direction and transfer to the CB of AVO. At this time, Cr(VI) will obtain photogenerated electrons and be reduced to Cr(III). Since the CB value of CN is −0.80 eV lower than the potential of $O_2/{}^{\bullet}O_2^{-}$ of −0.33 eV,[56] part of the photogenerated electrons convert the dissolved O_2 in the solution to $^{\bullet}O_2^{-}$, which reacts with Cr(VI) in the solution and reduces it to trivalent Cr(III). The following chemical equations for the reaction mechanism are presented:

$$\mathrm{Cr(VI)} + 3e^{-} \rightarrow \mathrm{Cr(III)}$$

$$O_2 + e^{-} \rightarrow {}^{\bullet}O_2^{-}$$

$$\mathrm{Cr(VI)} + 3{}^{\bullet}O_2^{-} \rightarrow \mathrm{Cr(III)} + 3O_2$$

4. Conclusion

In summary, 4AVO/CN/0.06DT ternary composites were synthesized by a two-step method. Through a series of characterization analyses, the crystal morphology, microstructure, optical properties and photoelectrochemical properties of the composites were determined. Taking Cr(VI) in aqueous solution as a target pollutant, the degradation efficiency of 4AVO/CN/0.06DT reached 70% within 60 min under visible light irradiation, far exceeding the degradation efficiency of the constituent pure substances. The cyclic performance test of the composite material showed that it still had a stable degradation effect after three cycles. The degradation efficiency in solution at different pH values was investigated. When the pH value of the solution gradually increased, the degradation efficiency gradually decreased, which was mainly caused by the different forms of Cr(VI) under different pH values. Diatomite provides a reaction site for Ag_3VO_4 and $g\text{-}C_3N_4$, and promotes the photoreduction of Cr(VI). This work provides a certain reference significance for the treatment of industrial heavy metal wastewater.

Conflicts of interest

There are no conflicts to declare.

Acknowledgements

The authors gratefully acknowledge financial support provided by the National Natural Science Foundation of China (no. 21201004, 81903859), Cultivation project of scientific research project reserve of Anhui Jianzhu University (no. 2020XMK01), 2014 Anhui Provincial Universities Excellent Young Talents Plan, National innovation project (no. C21001) and University-level innovation project of Anhui Jianzhu University (no. C21307).

References

1 H. Wenyuan, L. Ning, Z. Xiaodong, W. Minghong and T. Liang, *Appl. Surf. Sci.*, 2017, **425**, 107–116.
2 J. T. Juan, M. A. Grela and M. I. Litter, *Environ. Sci. Technol.*, 2004, **38**(5), 1589–1594.
3 W. Chong-Chen, D. Xue-Dong, L. Jin Li, G. Xin-Xing, W. Peng and Z. Jia, *Appl. Catal., B*, 2016, **193**, 198–216.
4 C. Guojun, H. Juncheng, M. Yang, Y. Huimin and Q. Liping, *Water Res.*, 2019, **148**, 10–18.
5 E. N. Zare, A. Motahari and M. Sillanpaa, *Environ. Res.*, 2018, **162**, 173–195.
6 Z. Wei, N. Zheng, X. Dong, X. Zhang, H. Ma, X. Zhang and M. Xue, *Chemosphere*, 2020, **257**, 127210–127219.
7 H. Sun and S.-J. Park, *Appl. Surf. Sci.*, 2020, **531**, 147325–147333.
8 Y. Xiao-Hong, M. Si-Qi, D. Xue-Dong, Z. Chen, F. Huifen, W. Peng and W. Chong-Chen, *Chem. Eng. J.*, 2019, **375**, 121944–121957.
9 R. Liang, F. F. Jing, L. J. Shen, N. Qin and L. Wu, *J. Hazard. Mater.*, 2015, **287**, 364–372.
10 W. Wang, Q. Niu, G. Zeng, C. Zhang, D. Huang, B. Shao, C. Zhou, Y. Yang, Y. Liu, H. Guo, W. Xiong, L. Lei, S. Liu, H. Yi, S. Chen and X. Tang, *Appl. Catal., B*, 2020, **273**, 119051–119064.

11 S. Ye, M. Yan, X. Tan, J. Liang, G. Zeng, H. Wu, B. Song, C. Zhou, Y. Yang and H. Wang, *Appl. Catal., B*, 2019, **250**, 78–88.

12 D. Lei, J. Xue, X. Peng, S. Li, Q. Bi, C. Tang and L. Zhang, *Appl. Catal., B*, 2021, **282**, 119578–119590.

13 P. Karthikeyan, K. Ramkumar, K. Pandi, A. Fayyaz, S. Meenakshi and C. M. Park, *Ceram. Int.*, 2021, **47**(3), 3692–3698.

14 A. F. Danil de Namor, A. El Gamouz, S. Frangie, V. Martinez, L. Valiente and W. Oliver A, *J. Hazard. Mater.*, 2012, **241–242**, 14–31.

15 G. Sriram, M. Kigga, U. Uthappa, R. M. Rego, V. Thendral, T. Kumeria, H.-Y. Jung and M. D. Kurkuri, *Adv. Colloid Interface Sci.*, 2020, **282**, 102198–102228.

16 S. E. Bailey, T. J. Olin, R. Mark Brick and D. Dean Adrian, *Water Res.*, 1999, **33**(11), 2469–2479.

17 Z. Sun, Z. Hu, Y. Yan and S. Zheng, *Appl. Surf. Sci.*, 2014, **314**, 251–259.

18 F. Haibo, R. Qifang, W. Sulei, J. Zhen and D. Yi, *J. Alloys Compd.*, 2019, **775**, 845–852.

19 Y. Du, X. Wang, J. Wu, C. Qi and Y. Li, *Particuology*, 2018, **40**, 123–130.

20 X. Zhang, J. Zhou, D. Yang, S. Chen, J. Huang and Z. Li, *Catal. Today*, 2019, **335**, 228–235.

21 Z. M. Sun, Y. Yan, G. X. Zhang, Z. Y. Wu and S. L. Zheng, *Adv. Powder Technol.*, 2015, **26**(2), 595–601.

22 X. Dong, B. Ren, X. Zhang, X. Liu, Z. Sun, C. Li, Y. Tan, S. Yang, S. Zheng and D. D. Dionysiou, *Appl. Catal., B*, 2020, **272**, 118971–118983.

23 X. Chunyu, R. Qifang, L. Xin, J. Zhen, D. Yi, Z. Haitao, L. Jinpeng and C. Ranran, *Appl. Surf. Sci.*, 2021, **543**, 148844–148855.

24 P. Tanniratt, T. Wasanapiarnpong, C. Mongkolkachit and P. Sujaridworakun, *Ceram. Int.*, 2016, **42**(15), 17605–17609.

25 X. Sun, H. Huang, Q. Zhao, T. Ma and L. Wang, *Adv. Funct. Mater.*, 2020, **30**(22), 1910005–1910048.

26 A. Mishra, A. Mehta, S. Basu, N. P. Shetti, K. R. Reddy and T. M. Aminabhavi, *Carbon*, 2019, **149**, 693–721.

27 P. Niu, L. Zhang, G. Liu and H.-M. Cheng, *Adv. Funct. Mater.*, 2012, **22**(22), 4763–4770.

28 S. Rao, Y. Li, H. Liu, S. Gao, J. Zhao, N. Rahman, J. Li, Y. Zhou, D. Wang, L. Zhang, Q. Liu and J. Yang, *Ceram. Int.*, 2021, **47**(6), 8528–8537.

29 J. Gong, C. Li and M. R. Wasielewski, *Chem. Soc. Rev.*, 2019, **48**(7), 1862–1864.

30 Y. Cui, Z. Ding, X. Fu and X. Wang, *Angew. Chem., Int. Ed.*, 2012, **51**(47), 11814–11818.

31 T. Sano, S. Tsutsui, K. Koike, T. Hirakawa, Y. Teramoto, N. Negishi and K. Takeuchi, *J. Mater. Chem. A*, 2013, **1**(21), 6489–6497.

32 F. Guo, M. Li, H. Ren, X. Huang, K. Shu, W. Shi and C. Lu, *Sep. Purif. Technol.*, 2019, **228**, 115770–115777.

33 W. Jiang, D. Qu, L. An, X. Gao, Y. Wen, X. Wang and Z. Sun, *J. Mater. Chem. A*, 2019, **7**(31), 18348–18356.

34 X. Shen, Y. Zhang, Z. Shi, S. Shan, J. Liu and L. Zhang, *J. Alloys Compd.*, 2021, **851**, 156743–156755.

35 N. Kumaresan, M. M. A. Sinthiya, M. Sarathbavan, K. Ramamurthi, K. Sethuraman and R. R. Babu, *Sep. Purif. Technol.*, 2020, **244**, 116356–116367.

36 L. Sun, J. Li, X. Li, C. Liu, H. Wang, P. Huo and Y. S. Yan, *J. Colloid Interface Sci.*, 2019, **552**, 271–286.

37 S. Li, S. Hu, W. Jiang, Y. Liu, J. Liu and Z. Wang, *J. Colloid Interface Sci.*, 2017, **501**, 156–163.

38 T. Zhu, Y. Song, H. Ji, Y. Xu, Y. Song, J. Xia, S. Yin, Y. Li, H. Xu, Q. Zhang and H. Li, *Chem. Eng. J.*, 2015, **271**, 96–105.

39 G. Fan, Z. Ma, X. Li and L. Deng, *Ceram. Int.*, 2021, **47**(4), 5758–5766.

40 Y. Tian, B. Chang, J. Lu, J. Fu, F. Xi and X. Dong, *ACS Appl. Mater. Interfaces*, 2013, **5**(15), 7079–7085.

41 K. S. Al-Namshah and R. M. Mohamed, *Ceram. Int.*, 2021, **47**(4), 5003–5012.

42 P. Yu, X. Zhou, Y. Yan, Z. Li and T. Zheng, *Colloids Surf., B*, 2019, **179**, 170–179.

43 P. T. Pitchaimani Veerakumar, L. King-Chuen and L. Shang-Bin, *ACS Sustainable Chem. Eng.*, 2017, **5**, 5302–5332.

44 A. Raja, P. Rajasekaran, B. Vishnu, K. Selvakumar, J. Yeon Do, M. Swaminathan and M. Kang, *Sep. Purif. Technol.*, 2020, **252**, 117446–117457.

45 P. Zhu, Y. Chen, M. Duan, M. Liu and P. Zou, *Powder Technol.*, 2018, **336**, 230–239.

46 J. Liu, T. Zhang, Z. Wang, G. Dawson and W. Chen, *J. Mater. Chem.*, 2011, **21**(38), 14398–14402.

47 F. Yuan, Z. Sun, C. Li, Y. Tan, X. Zhang and S. Zheng, *J. Hazard. Mater.*, 2020, **396**, 122694–122706.

48 W. Zhao, Y. Feng, H. Huang, P. Zhou, J. Li, L. Zhang, B. Dai, J. Xu, F. Zhu, N. Sheng and D. Y. C. Leung, *Appl. Catal., B*, 2019, **245**, 448–458.

49 S. M. Wang, Y. Guan, L. P. Wang, W. Zhao, H. He, J. Xiao, S. G. Yang and C. Sun, *Appl. Catal., B*, 2015, **168–169**, 448–457.

50 L. Cui, J. Song, A. F. McGuire, S. Kang, X. Fang, J. Wang, C. Yin, X. Li, Y. Wang and B. Cui, *ACS Nano*, 2018, **12**(6), 5551–5558.

51 L. Liu, T. Hu, K. Dai, J. Zhang and C. Liang, *Chin. J. Catal.*, 2021, **42**(1), 46–55.

52 F. Mei, K. Dai, J. Zhang, W. Li and C. Liang, *Appl. Surf. Sci.*, 2019, **488**, 151–160.

53 H. Xu, Z. Wu, M. Ding and X. Gao, *Mater. Des.*, 2017, **114**, 129–138.

54 Y. Li, Z. Liu, Y. Wu, J. Chen, J. Zhao, F. Jin and P. Na, *Appl. Catal., B*, 2018, **224**, 508–517.

55 F. Jing, R. Liang, J. Xiong, R. Chen, S. Zhang, Y. Li and L. Wu, *Appl. Catal., B*, 2017, **206**, 9–15.

56 Z. Long, G. Zhang, H. Du, J. Zhu and J. Li, *J. Hazard. Mater.*, 2021, **407**, 124394–124443.